International Journal of Colorectal Disease (2025) 40:129
https://doi.org/10.1007/s00384-025-04919-5

RESEARCH

Dual-energy CT combined with histogram parameters in the assessment of perineural invasion in colorectal cancer

Yuxuan Wang[1] · Huaqing Tan[1] · Shenglin LI[2] · Changyou Long[1] · Boqi Zhou[1] · Zhijie Wang[1] · Yuntai Cao[1]

Accepted: 13 May 2025

Abstract

Purpose The purpose is to evaluate the predictive value of dual-energy CT (DECT) combined with histogram parameters and a clinical prediction model for perineural invasion (PNI) in colorectal cancer (CRC).

Methods We retrospectively analyzed clinical and imaging data from 173 CRC patients who underwent preoperative DECT-enhanced scanning at two centers. Data from Qinghai University Affiliated Hospital ($n=120$) were randomly divided into training and validation sets, while data from Lanzhou University Second Hospital ($n=53$) served as the external validation set. Regions of interest (ROIs) were delineated to extract spectral and histogram parameters, and multivariate logistic regression identified optimal predictors. Six machine learning models—support vector machine (SVM), decision tree (DT), random forest (RF), logistic regression (LR), k-nearest neighbors (KNN), and extreme gradient boosting (XGBoost)—were constructed. Model performance and clinical utility were assessed using receiver operating characteristic (ROC) curves, calibration curves, and decision curve analysis (DCA).

Results Four independent predictive factors were identified through multivariate analysis: entropy, $CT40_{KeV}$, CEA, and skewness. Among the six classifier models, RF model demonstrated the best performance in the training set (AUC = 0.918, 95% CI: 0.862–0.969). In the validation set, RF outperformed other models (AUC = 0.885, 95% CI: 0.772–0.972). Notably, in the external validation set, the XGBoost model achieved the highest performance (AUC = 0.823, 95% CI: 0.672–0.945).

Conclusion Dual-energy CT-based combined with histogram parameters and clinical prediction modeling can be effectively used for preoperative noninvasive assessment of perineural invasion in colorectal cancer.

Keywords Machine learning · Colorectal neoplasms · Radiographic image interpretation · Computer-assisted

Introduction

Colorectal cancer (CRC) is one of the most prevalent malignant tumors in the digestive system, primarily involving the rectum and sigmoid colon, with the rectum being the most common site. According to statistics, CRC has the third highest incidence rate and the second highest mortality rate worldwide [1]. Despite significant advances in surgical techniques and adjuvant radiotherapy in recent years, the long-term survival rate of CRC patients remains unsatisfactory [2]. Perineural invasion (PNI), which refers to the invasion of tumor cells into neural structures and their spread along nerve sheaths, affects the tumor microenvironment and is an independent risk factor for recurrence and reduced survival [3]. Most studies have shown that the prevalence of PNI in patients with CRC ranges from 9 to 33% [4]. The National Comprehensive Cancer Network (NCCN) guidelines list PNI as a high-risk factor for colorectal cancer recurrence [1]. Clinical studies have demonstrated that patients with positive PNI exhibit more aggressive tumor biological behavior, with a significantly increased risk of local recurrence and a higher propensity for distant multiorgan metastases (including the liver, lungs, bones, brain, and distant lymph nodes) [5, 6]. Therefore, accurate preoperative assessment of PNI status

Yuxuan Wang and Huaqing Tan are co-frst author (author Yuxuan Wang and author Huaqing Tan contributed equally).

✉ Yuntai Cao
caoyuntai04@126.com

[1] Department of Radiology, Qinghai University Affiliated Hospital, Xining, China

[2] Department of Radiology, Sichuan Academy of Medical Sciences and Sichuan Provincial People's Hospital, Sichuan, China

Published online: 27 May 2025

holds significant clinical value in guiding treatment decisions, such as determining the optimal surgical resection extent and the need for neoadjuvant chemoradiotherapy (nCRT) or other multimodal therapeutic strategies.

Currently, the diagnosis of preoperative PNI mainly relies on invasive biopsy. However, biopsy samples can only reflect static information about localized lesions, which is difficult to fully represent tumor heterogeneity and may miss lesions with invasive properties [7]. Therefore, the development of noninvasive preoperative imaging techniques is essential to guide clinical decision-making. Enhanced CT is a routine preoperative tool for CRC patients and can provide information about the blood supply of the lesion. However, conventional CT imaging is limited in the accurate assessment of PNI, which cannot be effectively identified by features such as short-axis diameter, morphology, or borders [8]. Recent advances in imaging techniques have provided novel non-invasive methods for preoperative assessment of PNI. As a functional imaging technique, dual-energy CT (DECT) provides multi-energy information and quantitative parameters, such as single-energy images, substrate images, and energy-spectrum curves, which can better reflect tissue characteristics, increase vascular contrast, and reduce artifacts and radiation exposure, thus improving lesion detection rates [7–10]. Quantitative analysis of tumor characteristic parameters not only provides an objective basis for formulating individualized treatment plans but also enables dynamic monitoring during therapy, allowing timely adjustment of treatment strategies based on therapeutic response, thereby improving patient outcomes [11].

With the advancement of tumor imaging research, the application of texture analysis in evaluating tumor heterogeneity has gradually increased [1]. Histogram analysis, as an advanced medical image processing method, assesses tumor homogeneity and heterogeneity by analyzing the distribution and variation of gray-scale pixels in images to objectively characterize tumor tissues [12, 13]. Compared with higher-order texture features, histogram features demonstrate superior reproducibility and can reduce human subjective observation errors [1]. Several studies have confirmed the significant role of histogram parameters in predicting tumor prognosis–related factors [3].

In CRC research, while dual-energy CT scanning and histogram analysis have been applied separately in various studies, no research has investigated PNI prediction in CRC using DECT technology combined with histogram analysis methods. Therefore, this study aims to evaluate the predictive value of DECT combined with histogram parameters and clinical prediction models for PNI status in rectal cancer, which may provide a reference for developing personalized treatment plans and prognostic assessments.

Methods

Patients

This retrospective study complied with the Declaration of Helsinki and was approved by the Ethics Committees of Qinghai University Affiliated Hospital and Lanzhou University Second Hospital (approval nos. P-SL-2022–008 and 2022 A-298), with waived informed consent. Clinical and imaging data were collected from patients who underwent radical resection for pathologically confirmed colorectal cancer (CRC) between May 2020 and December 2023 at both institutions. Inclusion criteria: (1) postoperative pathological confirmation of PNI status; (2) preoperative dual-energy CT examination within 1 month before surgery; (3) no prior anti-tumor therapy before both surgery and CT scanning. Exclusion criteria: (1) preoperative imaging evidence of distant metastasis; (2) patients with concurrent malignant tumors at other sites; (3) incomplete clinical information or imaging data; and (4) poor image quality unsuitable for evaluation. The patient screening flowchart is presented in Fig. 1. From Qinghai University Affiliated Hospital, 120 eligible CRC patients were enrolled (75 males and 45 females; age range 30–85 years, mean age 61.08 ± 10.29 years), including 67 rectal cancers and 53 colon cancers. Pathological classification identified 65 PNI-positive and 55 PNI-negative cases, randomly allocated to training ($n = 84$) and validation ($n = 36$) sets at a 7:3 ratio. An additional 53 CRC patients (32 PNI-positive and 21 PNI-negative) from Lanzhou University Second Hospital served as an external validation cohort.

Image acquisition

All patients were placed in the supine position and underwent pelvic plain scanning followed by enhanced scanning using a GE Discovery CT 750 HD gemstone energy spectrum CT scanner. The scanning parameters were as follows: rapid tube voltage switching between 140 and 80 kV (switching time 0.5 ms) with automatic tube current adjustment; slice thickness 5 mm; pitch 0.984; rotation speed 0.6 s/r. The abdominal aortic monitoring trigger threshold was set at 150 HU, with GSI mode scans performed in arterial (5.4 s post-trigger) and venous (20 s post-trigger) phases, covering from the diaphragmatic apex to the pelvic floor. The contrast agent iopromide (320 mg I/mL) was administered intravenously at 3.0 mL/s using a CT dual-chamber high-pressure injector, with a total dose of 1.2 mL/kg body weight. Scanning phases were arterial (25–30 s), venous (60–70 s), and delayed (120–150 s). For optimal bowel distension, patients received appropriate

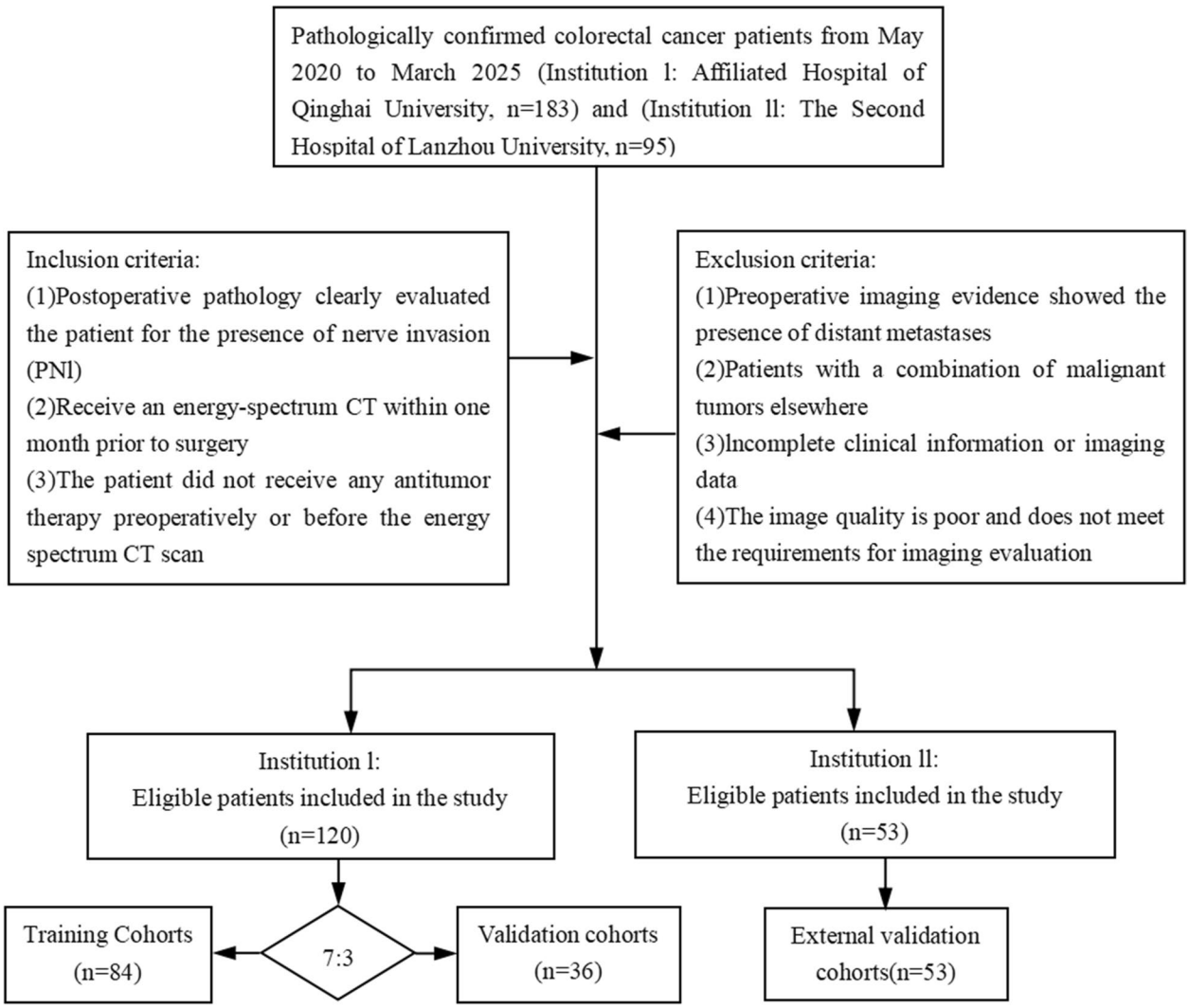

Fig. 1 Flow chart of patient screening

hypotonic contrast agent (1:1 mixture of coupling agent and water) via rectal administration prior to scanning to moderately dilate the intestinal lumen, reduce gas interference, and ensure image quality.

Image analysis

Standardization processing

This study integrated multicenter imaging data. To address potential image quality variations caused by differences in scanner models and parameters, we implemented the following standardization procedures: (1) prior to lesion delineation, all CT images were uniformly adjusted to a window width of 350 HU and window level of 40 HU to minimize inter-scanner HU value variations; (2) image resampling with unified voxel spacing (1mm × 1mm × 1 mm) to eliminate resolution discrepancies.

In portal venous phase CT images, the microcirculation characteristics of tumors are more pronounced, better reflecting the growth and blood supply of tumor neovascularization [7]. Therefore, we analyzed lesions using portal venous phase CT images. Two experienced attending radiologists (with 5 and 10 years of diagnostic experience, respectively) independently reviewed the images. Image processing was performed using a GE AW 4.7 workstation (GSI-viewer; GE Healthcare, Milwaukee, WI, USA), with monochromatic images at 70 keV evaluated by the Gemstone Spectral Imaging (GSI) Viewer software. Previous studies have demonstrated that 70 keV monochromatic images provide optimal sensitivity–specificity balance for abdominal lesion analysis [8]. Based on postoperative pathology findings, the primary radiologist placed a circular region of interest (ROI)

on the portal phase 70 keV monochromatic images, covering the lesion's largest dimension (mean area 96.78 mm^2, range 21.23–179.67 mm^2). ROIs were carefully positioned in highly enhanced tumor areas while avoiding obvious vasculature, cystic changes, calcifications, hemorrhage, and necrotic regions. The ROI of each lesion was measured three times with the mean value recorded (Fig. 2B, H). A second radiologist performed identical measurements. To minimize measurement bias, the results from both radiologists were averaged after consistency verification of raw data. Both reviewers were informed of the surgical tumor location but remained blinded to PNI status during analysis. Using GSI viewer software, we obtained (1) monochromatic CT values, (2) effective atomic number (Zeff), (3) iodine concentration (IC), and (4) water concentration (WC).The spectral curve slope (λ_{HU}) was calculated from virtual monochromatic images (40–70 keV) using the formula: $\lambda_{HU} = ([\text{CT value } \{40\text{ keV}\} - \text{CT value } \{70\text{ keV}\}]/30)$.

Histogram analysis

The two aforementioned physicians imported DICOM-format images into the FireVoxel software package (version 416 C; https://frevoxel.org/). On axial venous phase

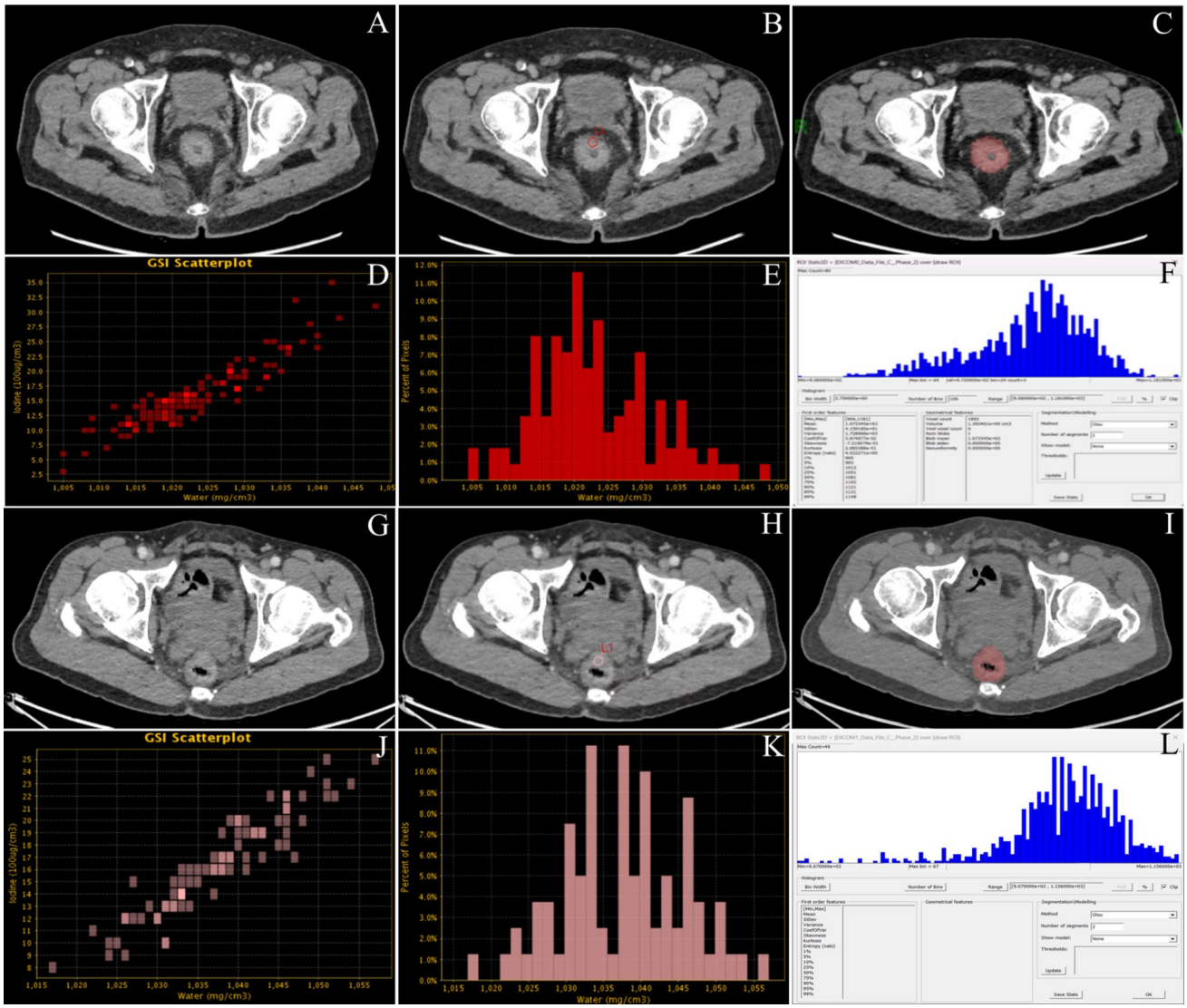

Fig. 2 **A**–**F** PNI group patient, male, 71 years old. **A** Portal venous phase dual-energy CT image of tumor; **B** ROIs outlined on spectral CT post-processing workstation; **C** ROIs marked at tumor's largest cross-section in FireVoxel software for histogram acquisition; **D** spectral ROI scatter plot; **E** tumor region grayscale histogram; **F** histogram parameters generated by FireVoxel software. **G**–**L** non-PNI group patient, male, 52 years old. **G** Portal venous phase dual-energy CT image of tumor. **H** ROIs outlined on spectral CT post-processing workstation. **I** ROIs marked at tumor's largest cross-section in FireVoxel software for histogram acquisition. **J** Spectral ROI scatter plot. **K** Tumor region grayscale histogram. **L** Histogram parameters generated by FireVoxel software

images, they manually outlined the maximum dimension ROI of rectal cancer lesions, carefully avoiding adjacent normal tissues and peritumoral edematous areas. Considering partial volume effects, ROIs were deliberately drawn slightly smaller than visible tumor boundaries [14], as illustrated in Fig. 2C,I. The software automatically generated grayscale histograms and calculated the following parameters: minimum, maximum, mean, standard deviation (SD), variance, coefficient of variation (CV), skewness, kurtosis, entropy, and 1 st–99 th percentiles (Fig. 2F, L). To assess interobserver reproducibility, a third radiologist with 10 years of pelvic CT experience independently reviewed the measurements.

Tumor markers and pathological evaluation

According to clinical diagnostic criteria, the following thresholds defined abnormal tumor markers in this study: CEA >5 ng/mL, CA125 >35 U/mL, and CA199 ≥ 37 U/mL; values below these thresholds were considered normal.

All rectal cancer patients underwent total mesorectal excision (TME), while colon cancer patients received complete mesorectal excision (CME). The resection specimens were evaluated within 1 week postoperatively by a senior pathologist blinded to patients' clinical and imaging data. Based on the WHO Classification of Tumors of the Digestive System (5 th edition) and AJCC Cancer Staging Manual (8 th edition), PNI was defined as a positive diagnosis when tumor cells were present in the peripheral nerve interspace and encircled at least one-third of the nerve circumference or infiltrated into any of the three layers of connective tissue sheaths encircling the nerve [15].

Statistical analysis

Statistical analysis was performed using SPSS 28.0 and R software (version 4.1.3). Continuous variables with normal distribution were analyzed using independent samples *t* test and expressed as mean ± standard deviation, while non-normally distributed data were analyzed using Mann–Whitney *U* test and presented as median (Q1, Q3). Categorical variables were expressed as frequencies and percentages (%), with between-group comparisons made using chi-square test. Univariate analysis was first conducted using independent-samples *t* test or chi-square test to screen for statistically significant variables ($P < 0.05$). Subsequently, multivariate logistic regression analysis was performed on statistically significant variables to identify independent predictors. In all statistical analyses, $P < 0.05$ was considered statistically significant.

Predictive modeling and evaluation

Potential predictors were initially screened through univariate and multivariate logistic regression analyses. Six classification models were subsequently constructed: support vector machine (SVM), decision tree (DT), random forest (RF), logistic regression (LR), k-nearest neighbors (KNN), and XGBoost. Model performance was evaluated using receiver operating characteristic (ROC) curves with area under the curve (AUC) calculations for training, validation, and external validation sets. Calibration curves assessed prediction accuracy, while decision curve analysis (DCA) evaluated clinical utility by measuring net benefit across various thresholds. Comprehensive evaluation incorporated accuracy, sensitivity, specificity, positive predictive value (PPV), negative predictive value (NPV), and F1-score.

Results

Baseline information and screening process of PNI predictors

This study included a total of 120 colorectal cancer (CRC) patients, with 84 cases in the training set (52 males, 32 females), mean age 61.05 ± 10.28 years and 36 cases in the validation set (23 males, 13 females), mean age 60.03 ± 10.09 years. During feature selection, potential PNI predictors were first screened through univariate analysis, with results showing that CEA, skewness, kurtosis, entropy, monochromatic CT value at 40 keV ($CT40_{keV}$), monochromatic CT value at 70 keV ($CT70_{keV}$), iodine concentration (IC), and effective atomic number (Zeff) were significantly associated with PNI (Table 1). Further multivariate logistic regression analysis (Table 2) using the stepwise forward method ultimately identified entropy, $CT40_{keV}$, skewness, and CEA as independent predictors of PNI. We employed the LightGBM model for feature selection and importance ranking, generating a feature importance bar chart and AUC trend line plot with confidence interval shading (fill_between), as shown in Fig. 3. Additionally, Boruta algorithm was applied to rank the importance of all features (see Supplementary Fig. 1). Both machine learning classifier feature selection methods demonstrated that the features obtained through multivariate screening exhibited high stability. SHAP analysis further elucidated the importance of these features in the multivariate model and their contribution to the model output (Fig. 4).

Construction of prediction models

Based on four features including entropy, $CT40_{keV}$, skewness, and CEA, we constructed six classifier models:

Table 1 Baseline information

Characteristic	PNI(-), $N = 55$	PNI(+), $N = 65$	p value[a]
Sex, *n* (%)			0.603
0	22 (40%)	23 (35%)	
1	33 (60%)	42 (65%)	
Age, median (IQR)	62.00 (54.00, 68.00)	64.00 (55.00, 70.00)	0.677
tumor_site, *n* (%)			0.398
0	22 (40%)	31 (48%)	
1	33 (60%)	34 (52%)	
CEA, *n* (%)			< 0.001
0	40 (73%)	20 (31%)	
1	15 (27%)	45 (69%)	
CA125, n (%)			0.718
0	43 (78%)	49 (75%)	
1	12 (22%)	16 (25%)	
CA199, *n* (%)			0.269
0	43 (78%)	45 (69%)	
1	12 (22%)	20 (31%)	
Minimum, median (IQR)	903.00 (821.00, 940.50)	918.00 (784.00, 943.00)	0.624
Maximum, median (IQR)	1,164.00 (1,146.50, 1,188.00)	1,172.00 (1,148.00, 1,189.00)	0.901
Mean, median (IQR)	1,079.65 (1,070.00, 1,090.00)	1,080.00 (1,070.00, 1,090.98)	0.762
SD, median (IQR)	35.98 (31.89, 45.38)	37.10 (30.22, 43.40)	0.628
Variance, median (IQR)	1,292.19 (1,016.62, 2,059.70)	1,364.63 (910.92, 1,880.00)	0.628
CV, median (IQR)	0.03 (0.03, 0.04)	0.03 (0.03, 0.04)	0.606
Skewness, median (IQR)	− 1.40 (− 1.93, − 1.13)	− 1.11 (− 1.67, − 0.86)	0.015
Kurtosis, median (IQR)	2.02 (1.50, 3.41)	1.11 (0.71, 1.60)	< 0.001
Entropy, median (IQR)	3.84 (3.62, 4.02)	4.51 (4.16, 4.64)	< 0.001
Perc.01, median (IQR)	961.00 (934.00, 993.50)	967.00 (948.00, 988.00)	0.428
Perc.05, median (IQR)	1,011.00 (983.00, 1,030.00)	1,012.00 (989.00, 1,032.00)	0.505
Perc.10, median (IQR)	1,035.00 (1,016.50, 1,050.00)	1,035.00 (1,015.00, 1,048.00)	0.856
Perc.25, median (IQR)	1,063.00 (1,054.50, 1,076.00)	1,060.00 (1,050.00, 1,075.00)	0.778
Perc.50, median (IQR)	1,083.00 (1,077.50, 1,096.50)	1,086.00 (1,076.00, 1,098.00)	0.904
Perc.75, median (IQR)	1,105.00 (1,092.00, 1,113.00)	1,103.00 (1,093.00, 1,118.00)	0.893
Perc.90, median (IQR)	1,117.00 (1,106.50, 1,129.00)	1,120.00 (1,107.00, 1,134.00)	0.649
Perc.95, median (IQR)	1,126.00 (1,115.00, 1,139.00)	1,127.00 (1,115.00, 1,143.00)	0.607
Perc.99, median (IQR)	1,141.00 (1,131.00, 1,159.00)	1,144.00 (1,128.00, 1,160.00)	> 0.999
$CT40_{keV}$, median (IQR)	191.76 (174.47, 213.64)	166.67 (149.40, 176.99)	< 0.001
$CT70_{keV}$, median (IQR)	72.88 (69.34, 80.18)	69.35 (62.82, 75.87)	0.005
HU, median (IQR)	3.38 (3.14, 3.96)	3.30 (2.97, 3.58)	0.127
IC, median (IQR)	18.28 (16.99, 21.40)	16.64 (14.95, 18.53)	< 0.001
WC, median (IQR)	1,028.91 (1,021.53, 1,036.20)	1,027.67 (1,019.72, 1,034.09)	0.662
Zeff, median (IQR)	8.66 (8.60, 8.82)	8.60 (8.52, 8.71)	0.012

CV coefficient of variation, *IC* iodine concentration, *PNI* perineural invasion, *SD* standard deviation, λ_{HU} slope of the spectral curve, *WC* water concentration, *Zeff* effective atomic number, *Perc.01–99* 1 st–99 th percentiles.

[a]Pearson's chi-squared test; Wilcoxon rank sum test; continuous variables are presented as median (Q1, Q3), while categorical variables are expressed as percentages [n (%)]. For tumor marker levels: CEA (> 5 ng/mL = 1, ≤ 5 ng/mL = 0), CA125 (> 35 U/mL = 1, ≤ 35 U/mL = 0), and CA199 (≥ 37 U/mL = 1, < 37 U/mL = 0).

support vector machine (SVM), decision tree (DT), random forest (RF), logistic regression (LR), K-nearest neighbors (KNN), and XGBoost. In the training set, the AUC values of these models ranged from 0.672 to 0.918, with RF performing best (AUC = 0.918, 95%CI: 0.862–0.969); in the validation set, the AUC values ranged from 0.695

Table 2 Results of multifactor logistic screening

Variables	B	*p* value	OR	(95%) CI	
				Lower limit	Upper limit
Entropy	11.807	< 0.001	134,193.823	360.962	49,888,862.97
$CT40_{KeV}$	− 0.034	0.035	0.966	0.936	0.998
CEA	− 1.726	0.032	0.178	0.037	0.859
Skewness	− 2.912	< 0.001	0.054	0.012	0.245

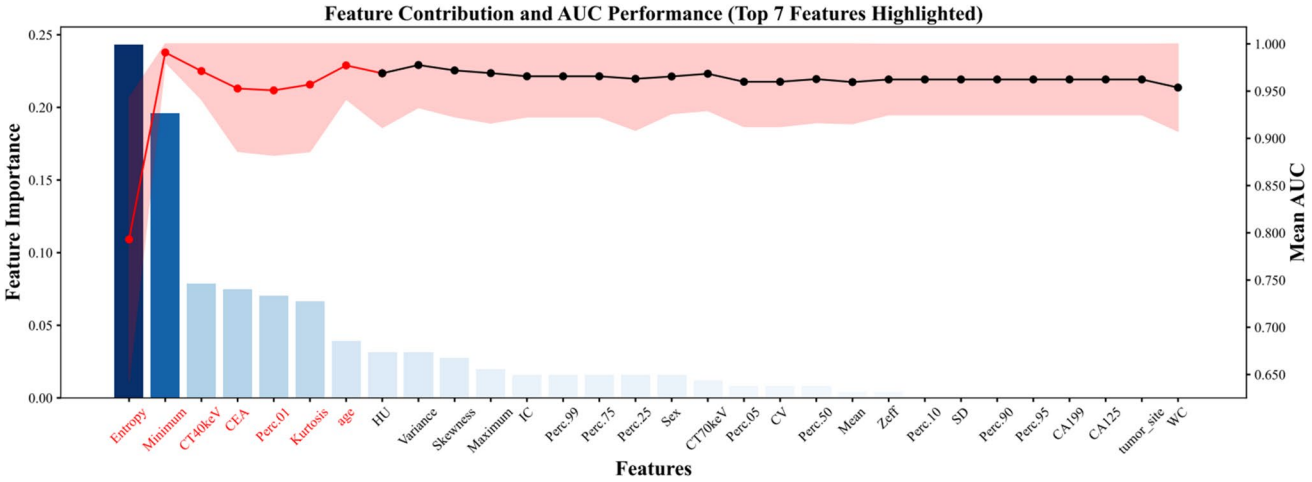

Fig. 3 Visualization of feature contributions and AUC performance highlighting key characteristics

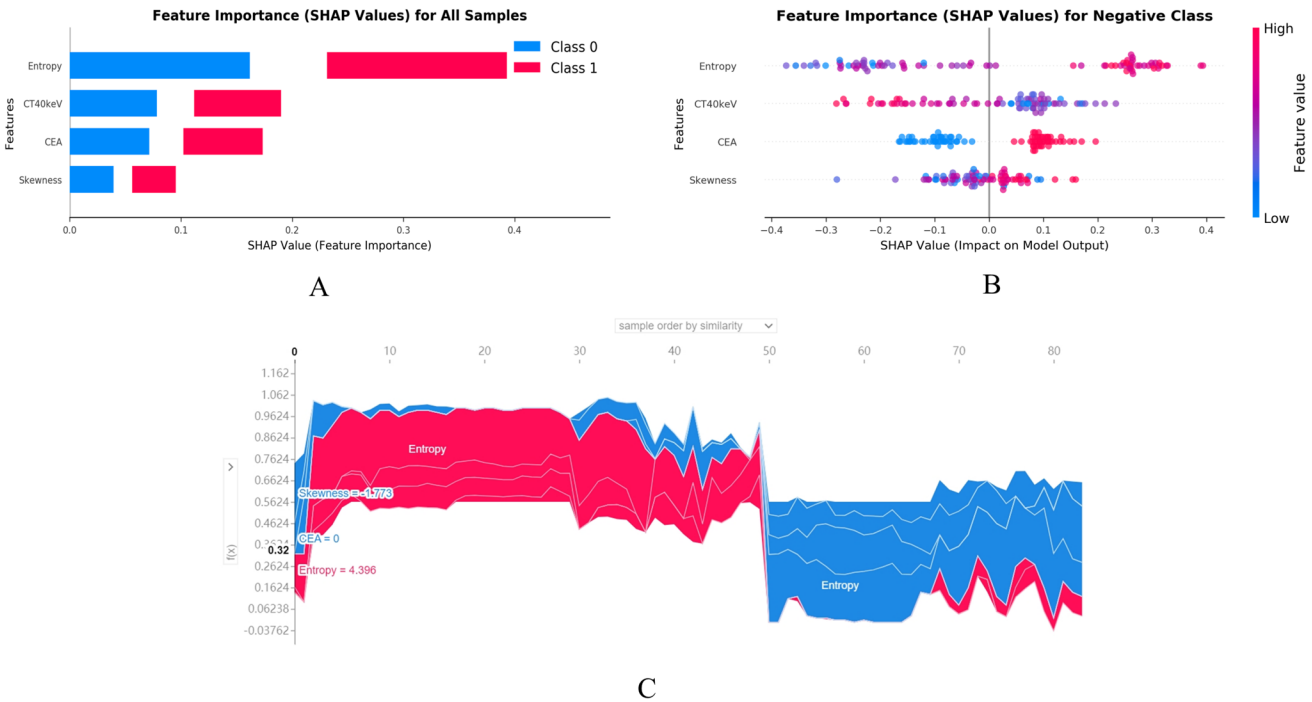

Fig. 4 SHAP analysis of feature importance and individual contribution of PNI predictors; **A** importance of each feature for PNI prediction, differentiated by category (class 1 and class 0); **B** distribution of feature SHAP values for PNI-negative patients, showing the direction and magnitude of the influence of the feature values on the model output; **C** waterfall plot demonstrating cumulative contribution of the features to the prediction for each patient

to 0.885, with RF classifier showing optimal performance (AUC = 0.885, 95%CI: 0.772–0.972); in the external validation set, the AUC values ranged from 0.731 to 0.823, with XGBoost model significantly outperforming other models (AUC = 0.823, 95%CI: 0.672–0.945). To visually evaluate the predictive performance, we plotted ROC curves for the training set, validation set, and external validation set (Fig. 5A–C), and the performance comparison of different models across datasets is shown in Fig. 6.The clinical utility of the model was further evaluated through decision curve analysis (DCA) (Fig. 5G–I). Results demonstrated that in the validation set, when the decision threshold probability ranged between 63 and 87%, the clinical prediction model incorporating dual-energy CT and histogram features showed greater net benefit compared to both "treat-all" and "treat-none" strategies, suggesting its potential for clinical decision support. Calibration performance is shown in Supplementary Fig. 2. Model stability was verified using five-fold cross-validation (results in Fig. 5D–F), with additional classifiers' cross-validation results provided in Supplementary Fig. 3. The confusion matrix for logistic regression appears in Supplementary Fig. 4. Feature robustness was assessed via bar charts of XGB classifier's feature sensitivity analysis using external data (Supplementary Fig. 5). To better understand model limitations, we analyzed misclassified cases to examine classification patterns and feature differences across datasets (Supplementary Fig. 6).

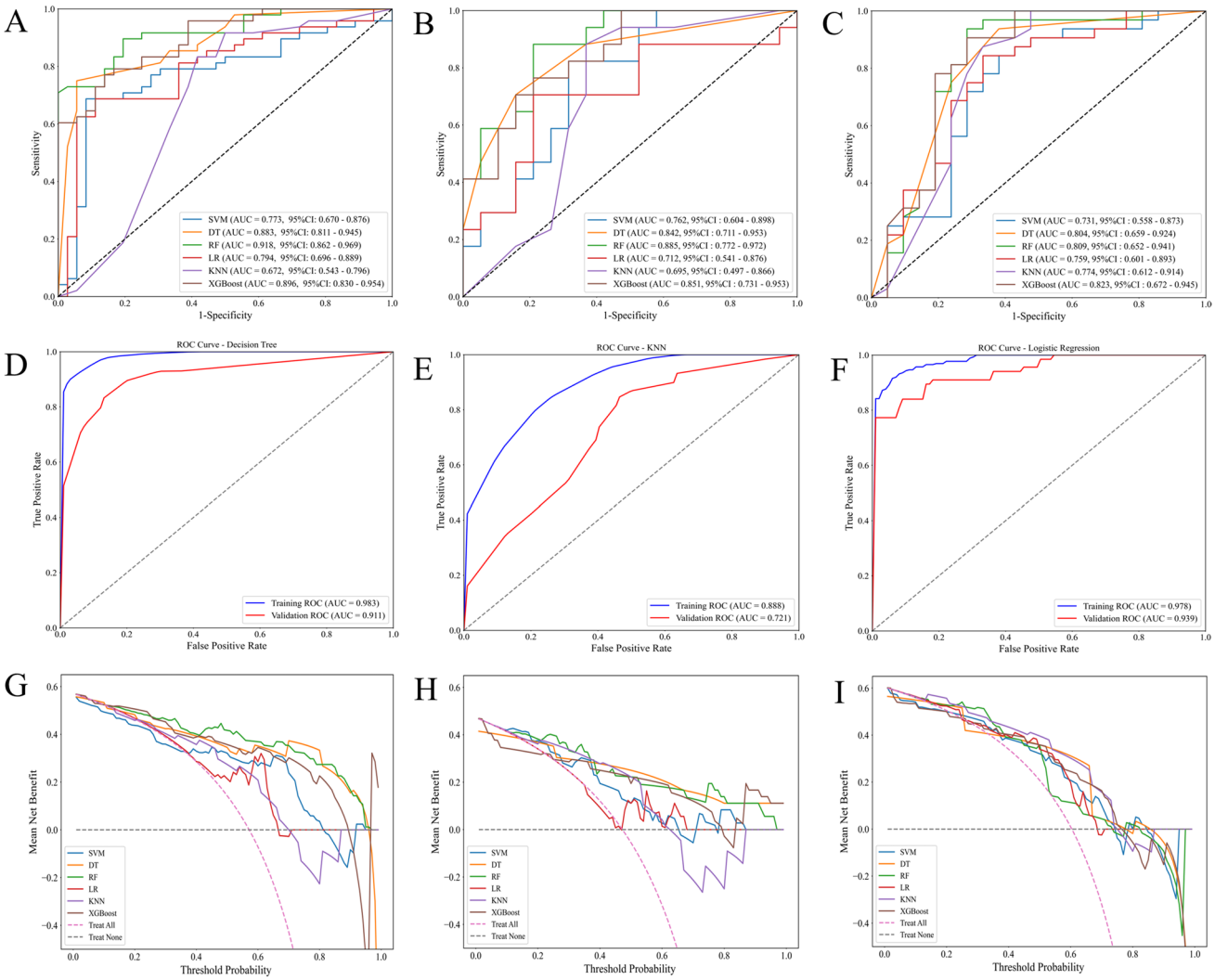

Fig. 5 **A–C** Receiver operating characteristic (ROC) curves for the training set, validation set, and external validation set, respectively; **D–F** comparison of the five-fold cross-validated ROC performance of decision tree (DT), K-nearest neighbors (KNN), and logistic regression (LR) models between the training and validation sets; **G–I** decision curve analysis (DCA) for each model across the training set, validation set, and external validation set

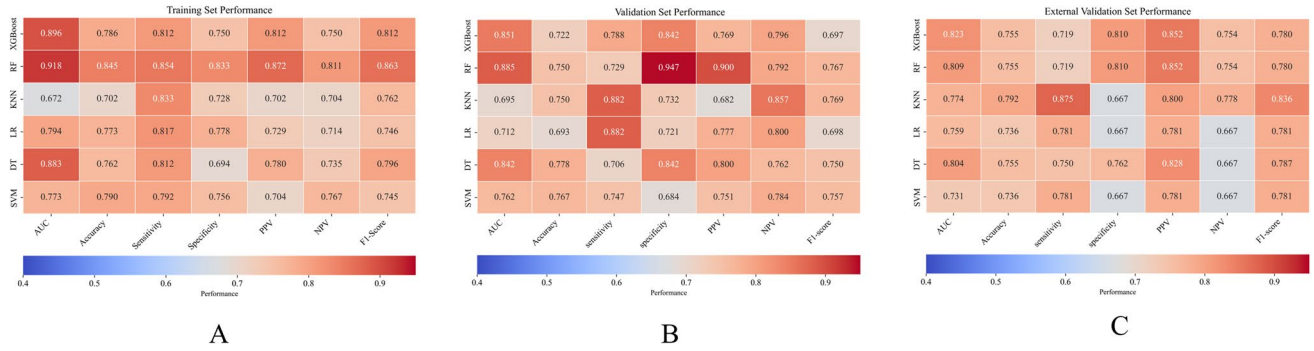

Fig. 6 The model performance of each classifier model in the training set (**A**), validation set (**B**), and external validation set (**C**)

Discussion

Colorectal cancer (CRC) is one of the most common gastrointestinal malignancies, with its global incidence steadily increasing in recent years, posing a significant threat to public health. While traditional research has primarily focused on vascular and lymphatic spread, perineural invasion (PNI) has emerged as an important alternative metastatic pathway [15]. Liebig et al. reported significantly higher 5-year disease-free survival rates in PNI-negative compared to PNI-positive patients (65% vs. 16%) [16]. Furthermore, PNI-positive CRC patients demonstrate relatively improved prognosis following neoadjuvant chemotherapy [1]. However, current PNI diagnosis depends on pathological biopsy, which suffers from considerable variability and standardization issues, leading to low detection rates [17].

With the advancement of imaging technology, non-invasive imaging modalities have been widely adopted in CRC clinical practice. Dual-energy computed tomography (DECT), renowned for its superior image quality and multi-parameter quantitative capabilities, has demonstrated promising outcomes across various disease studies. This study aimed to assess the feasibility and validity of a clinical prediction model integrating DECT with histogram parameters for preoperative non-invasive prediction of CRC PNI.

Through univariate analysis and multivariate logistic regression, this study identified entropy, $CT40_{KeV}$, skewness, and CEA as independent predictors for PNI. Based on these factors, we constructed six classifier models: support vector machine (SVM), decision tree (DT), random forest (RF), logistic regression (LR), K-nearest neighbors (KNN), and XGBoost and evaluated their predictive performance in the training set, validation set, and external validation set. The results showed the following: in the training set, the RF classifier performed best (AUC = 0.918, 95%CI: 0.862–0.969); in the validation set, the RF classifier achieved optimal performance (AUC = 0.885, 95%CI: 0.772–0.972); in the external validation set, the XGBoost model significantly outperformed other models with an AUC of 0.823 (95%CI: 0.672–0.945). These findings demonstrate that the predictive model based on portal venous phase DECT combined with multiparametric histogram analysis exhibits good predictive capability for preoperative PNI assessment.

Further calibration curve analysis demonstrated good calibration for all classifier models in both training and validation sets, indicating strong agreement between model predictions and actual outcomes. Decision curve analysis (DCA) revealed that when the threshold probability ranged from 63 to 87%, the DECT-based predictive models incorporating histogram parameters provided greater net benefit than both treat-all and treat-none strategies, confirming their clinical utility for decision-making. These results underscore the value of DECT combined with histogram analysis in supporting clinical decisions.

In the quantitative parameter analysis, entropy, $CT40_{keV}$, skewness, and CEA demonstrated significant predictive value. The results confirmed CEA as an independent PNI predictor, aligning with previous studies [18, 19] that established associations between elevated serum CEA levels and PNI positivity. Following literature evidence [18] of a nonlinear relationship between continuous CEA values and PNI status, we adopted the clinical standard 5 ng/mL as the CEA cutoff threshold. While CEA remains a clinically valuable tumor marker, its standalone predictive capacity for PNI risk shows limitations [20]. Our combined predictive model integrating radiomic features with clinical indicators exhibited superior discriminative performance in PNI risk assessment. The 40-keV monochromatic CT value holds particular diagnostic significance during venous phase imaging, approaching the k-edge energy level of iodine (33.2 keV) and demonstrating high diagnostic accuracy [21, 22]. Quantitative parameters in PNI-positive group showed lower values than the negative group, potentially attributable to tumor hypovascularity-induced liquefactive necrosis during PNI progression, manifesting as hypodense imaging features [23, 24]. Tumor tissue heterogeneity presents challenges for imaging analysis. While quantitative CT analysis reflects average tissue characteristics within the region of

interest (ROI), histogram analysis statistically characterizes voxel gray-level distribution, providing better assessment of intratumoral heterogeneity [1]. This study revealed significant differences in skewness between PNI-positive and PNI-negative groups ($p < 0.05$), demonstrating its predictive value for PNI status. As a key histogram feature, skewness quantitatively evaluates tumor gray-level intensity distribution asymmetry and serves as an important heterogeneity indicator [25]. Clinicopathological mechanisms suggest elevated skewness has multiple implications: (1) histologically correlating with reduced tumor differentiation and higher malignancy; (2) cellularly reflecting disarrangement from epithelial polarity loss; (3) biologically indicating increased heterogeneity, enhanced invasiveness, and accelerated growth/metastatic potential [26, 27]. Although whole-tumor histogram analysis comprehensively assesses heterogeneity, its complexity limits clinical utility [14]. Our largest cross-section–based method offers simpler, more efficient clinical application despite potential information loss. Entropy, reflecting voxel gray-scale distribution randomness, was significantly higher in PNI-positive patients, supporting its predictive potential [3].

This study has the following main limitations: First, constrained by the single-center research design, the sample size is relatively insufficient, and subsequent multicenter collaboration is needed to expand the sample size to validate the model's generalization ability. Second, manually delineating tumor ROIs is time-consuming, and automatic segmentation methods are not yet mature enough, requiring further improvement to enhance efficiency. Additionally, although DECT combined with histogram parameters demonstrates good predictive ability for PNI, its reliability as a substitute for pathological diagnosis still needs to be confirmed through larger-scale prospective studies. Based on the current research findings, we suggest that follow-up work could delve into the following aspects: (1) integrating radiomics and deep learning technologies to construct a multi-scale feature analysis framework; (2) establishing standardized large-sample cohorts; (3) systematically exploring the quantitative association patterns between texture feature spatial distribution and PNI, with the aim of developing a more precise imaging prediction system for rectal cancer perineural invasion.

In conclusion, the clinical prediction model constructed in this study based on portal phase DECT and histogram parameters has significant value in the preoperative noninvasive assessment of PNI status in CRC. DECT multiparametric images can be acquired simultaneously with conventional enhanced CT without increasing radiation exposure or economic burden for patients [28]. Histogram analysis provides more in-depth quantitative information about the imaging data, thus enhancing its clinical application. Although the preliminary results are encouraging, future research needs to expand the sample size to optimize the model, ensuring its effectiveness and practicality in clinical practice.

Supplementary Information The online version contains supplementary material available at https://doi.org/10.1007/s00384-025-04919-5.

Author contribution All authors contributed to the conception and design of the study. Authors Yuxuan Wang and Huaqing Tan contributed equally. Material preparation, data collection, and analysis were performed by Yuxuan Wang, Huaqing Tan, Shenglin Li, Changyou Long, Boqi Zhou, and Zhijie Wang. The first draft of the manuscript was written by Yuxuan Wang and Huaqing Tan, and revised and refined by Yuntai Cao. All authors provided feedback on previous versions of the manuscript and reviewed the final version.

Funding This work was supported by the National Natural Science Foundation of China (No. 82260346), Qinghai Province "Kunlun Talents High-end Innovation and Entrepreneurial Talents" Top Talent Cultivation Project (No. 13,2021), Qinghai Provincial Department of Science and Technology of China (No. 2023-ZJ-918 M), and West Light Foundation of the Chinese Academy of Sciences (2024-1-14).

Data availability No datasets were generated or analysed during the current study.

Declarations

Ethics approval and consent to participate This retrospective study followed the ethical principles of the Declaration of Helsinki and was approved by the Ethics Committees of the Affiliated Hospital of Qinghai University and Lanzhou University Second Hospital (Approval No. P-SL-2022–008 and 2022 A-298), which exempted subjects from informed consent.

Consent to participate Informed consent was obtained from all individual participants included in the study.

Consent for publication The authors affirm that human research participants provided informed consent for publication of the images in Fig. 2.

Conflict of interest The authors declare no competing interests.

References

1. He R, Song G, Fu J, Dou W, Li A, Chen J (2024) Histogram analysis based on intravoxel incoherent motion diffusion-weighted

imaging for determining the perineural invasion status of rectal cancer. Quant Imaging Med Surg 14(8):5358–5372
2. Li S, Yuan L, Yue M et al (2023) Early evaluation of liver metastasis using spectral CT to predict outcome in patients with colorectal cancer treated with FOLFOXIRI and bevacizumab. Cancer Imaging 23(1):30
3. Wan L, Peng W, Zou S et al (2022) Predicting perineural invasion using histogram analysis of zoomed EPI diffusion-weighted imaging in rectal cancer. Abdom Radiol (NY) 47(10):3353–3363
4. Wang H, Huo R, He K et al (2024) Perineural invasion in colorectal cancer: mechanisms of action and clinical relevance. Cell Oncol (Dordr) 47(1):1–17
5. Zhang K, Ren Y, Xu S, Lu W, Xie S, Qu J et al (2021) A clinical-radiomics model incorporating T2-weighted and diffusion-weighted magnetic resonance images predicts the existence of lymphovascular invasion/perineural invasion in patients with colorectal cancer. Med Phys 48(9):4872–4882. https://doi.org/10.1002/mp.15001
6. Wan T, Cai G, Gao S, Feng Y, Huang H, Liu L et al (2021) Preoperative evaluation of perineural invasion in cervical cancer: development and independent validation of a novel predictive nomogram. Front Oncol 11:774459. https://doi.org/10.3389/fonc.2021.774459
7. Chen J, Ni L, Gong J et al (2024) Quantitative parameters of dual-layer spectral detector computed tomography for evaluating differentiation grade and lymphovascular and perineural invasion in colorectal adenocarcinoma. Eur J Radiol 178:111594
8. Cao Y, Zhang J, Bao H et al (2021) Development of a nomogram combining clinical risk factors and dual-energy spectral CT parameters for the preoperative prediction of lymph node metastasis in patients with colorectal cancer. Front Oncol 11:689176
9. Kato T, Uehara K, Ishigaki S et al (2015) Clinical significance of dual-energy CT-derived iodine quantification in the diagnosis of metastatic LN in colorectal cancer. Eur J Surg Oncol 41:1464–1470
10. Gong HX, Zhang KB, Wu LM et al (2016) Dual energy spectral CT imaging for colorectal cancer grading: a preliminary study. PLoS ONE 11:e0147756
11. Liu J, Sun L, Zhao X, Lu X (2023) Development and validation of a combined nomogram for predicting perineural invasion status in rectal cancer via computed tomography-based radiomics. J Cancer Res Ther 19(6):1552–1559. https://doi.org/10.4103/jcrt.jcrt_2633_22
12. Liu X, Han T, Wang Y, Liu H, Huang X, Zhou J (2023) Differentiating angiomatous meningioma from atypical meningioma using histogram analysis of apparent diffusion coefficient maps. Quant Imaging Med Surg 13(7):4160–4170
13. Zhang B, Zhou F, Zhou Q et al (2023) Whole-tumor histogram analysis of multi-parametric MRI for differentiating brain metastases histological subtypes in lung cancers: relationship with the Ki-67 proliferation index. Neurosurg Rev 46(1):218
14. Xue C, Zhou Q, Zhang P et al (2023) MRI histogram analysis of tumor-infiltrating CD8+ T cell levels in patients with glioblastoma. Neuroimage Clin 37:103353
15. Betge J, Langner C (2011) Vascular invasion, perineural invasion, and tumour budding: predictors of outcome in colorectal cancer. Acta Gastroenterol Belg 74(4):516–529
16. Liebig C, Ayala G, Wilks J et al (2009) Perineural invasion is an independent predictor of outcome in colorectal cancer. J Clin Oncol 27(31):5131–5137
17. Yuan X, Quan X, Che XL et al (2023) Preoperative prediction of the lymphovascular tumor thrombus of colorectal cancer with the iodine concentrations from dual-energy spectral CT. BMC Med Imaging 23(1):103
18. Huang Y, He L, Dong D, Yang C, Liang C, Chen X et al (2018) Individualized prediction of perineural invasion in colorectal cancer: development and validation of a radiomics prediction model. Chin J Cancer Res 30(1):40–50. https://doi.org/10.21147/j.issn.1000-9604.2018.01.05
19. Park IJ, Choi GS, Lim KH, Kang BM, Jun SH (2009) Serum carcinoembryonic antigen monitoring after curative resection for colorectal cancer: clinical significance of the preoperative level. Ann Surg Oncol 16(11):3087–3093. https://doi.org/10.1245/s10434-009-0625-z
20. Royston P, Moons KG, Altman DG, Vergouwe Y (2009) Prognosis and prognostic research: developing a prognostic model. BMJ 338:b604. https://doi.org/10.1136/bmj.b604
21. Nagayama Y, Iyama A, Oda S et al (2019) Dual-layer dual-energy computed tomography for the assessment of hypovascular hepatic metastases: impact of closing k-edge on image quality and lesion detectability. Eur Radiol 29(6):2837–2847
22. Bunch PM, Pavlina AA, Lipford ME, Sachs JR (2021) Dual-energy parathyroid 4D-CT: improved discrimination of parathyroid lesions from thyroid tissue using noncontrast 40-keV virtual monoenergetic images. AJNR Am J Neuroradiol 42(11):2001–2008
23. Chen WB, Shi QQ, Li ZM, Li ZY, Kang LQ (2022) Diagnostic value of spiral CT energy spectrum imaging in lymph node metastasis of colorectal cancer. Int J Colorectal Dis 37(9):2021–2029
24. Liu J, Pan H, Lin Q et al (2023) Added value of spectral parameters in diagnosing metastatic lymph nodes of pT1-2 rectal cancer. Abdom Radiol (NY) 48(4):1260–1267
25. Liu X, Huang X, Han T, Li S, Xue C, Deng J et al (2022) Discrimination between microcystic meningioma and atypical meningioma using whole-lesion apparent diffusion coefficient histogram analysis. Clin Radiol 77(11):864–869. https://doi.org/10.1016/j.crad.2022.07.004
26. Liu L, Liu Y, Xu L, Li Z, Lv H, Dong N et al (2017) Application of texture analysis based on apparent diffusion coefficient maps in discriminating different stages of rectal cancer. J Magn Reson Imaging 45(6):1798–1808. https://doi.org/10.1002/jmri.25460
27. Peng Y, Tang H, Meng X, Shen Y, Hu D, Kamel I et al (2020) Histological grades of rectal cancer: whole-volume histogram analysis of apparent diffusion coefficient based on reduced field-of-view diffusion-weighted imaging. Quant Imaging Med Surg 10(1):243–256. https://doi.org/10.21037/qims.2019.11.17
28. Li Q, Hong R, Zhang P et al (2024) A clinical-radiomics nomogram based on spectral CT multi-parameter images for preoperative prediction of lymph node metastasis in colorectal cancer. Clin Exp Metastasis 41(5):639–53